Frequency-Dependent Characteristics of Microstrip Discontinuities in Millimeter-Wave Integrated Circuits

PISTI B. KATEHI AND NICÓLAOS G. ALEXOPOULOS, SENIOR MEMBER, IEEE

***Abstract*—A theoretical approach for the representation of microstrip discontinuities by equivalent circuits with frequency-dependent parameters is presented. The model accounts accurately for the substrate presence and associated surface-wave effects, strip finite thickness, and radiation losses. The method can also be applied for the solution of microstrip components in the millimeter frequency range.**

I. Introduction

THE LITERATURE on the theory of microstrip lines and microstrip discontinuities is extensive but, almost without exception, the published methods do not account for radiation and discontinuity dispersion effects. Microstrip discontinuity modeling was initially carried out either by quasi-static methods [1]–[12] or by an equivalent waveguide model [13]–[22]. The former approach gives a rough estimate of the discontinuity parameters valid at low frequencies, while the latter gives some information about dispersion effects at higher frequencies. However, the applicability of the latter model is also of limited value since it does not account for losses due to radiation and surface-wave excitation at the microstrip discontinuity under investigation. Therefore, it is reasonable to assume that the data obtained with this model are accurate only at the lower frequency range, i.e., before radiation losses become significant.

In this paper, three types of microstrip discontinuities are presented by equivalent circuits with frequency-dependent parameters (see Fig. 1). The implemented method accounts accurately for all the physical effects involved including surface-wave excitation [23], [24]. The model developed in this paper also accounts for conductor thickness and it assumes that the transmission-line and resonator widths are much smaller than the wavelength. The latter assumption insures that the error incurred by neglecting the transverse vector component of the current distribution on each conducting strip is a second-order effect. For each type of discontinuity, the method of moments is applied to determine the current distribution in the longitudinal direction, while the longitudinal current dependence in the transverse direction is chosen to satisfy the edge condition at the effective width location [28]. Upon determining the current distribution, transmission-line theory is invoked to evaluate the elements of the admittance matrix for the open-end and the gap discontinuities (Fig. 1(a) and (b)). The same method is also applied for evaluation of the resonant frequency of the coupled microstrip resonator (Fig. 1(c)). The equivalent circuits for the first two discontinuities are evaluated and compared with the results obtained by a quasi-static method based on the concept of excess length and equivalent capacitance. Although the quasi-static model does not include the discon-

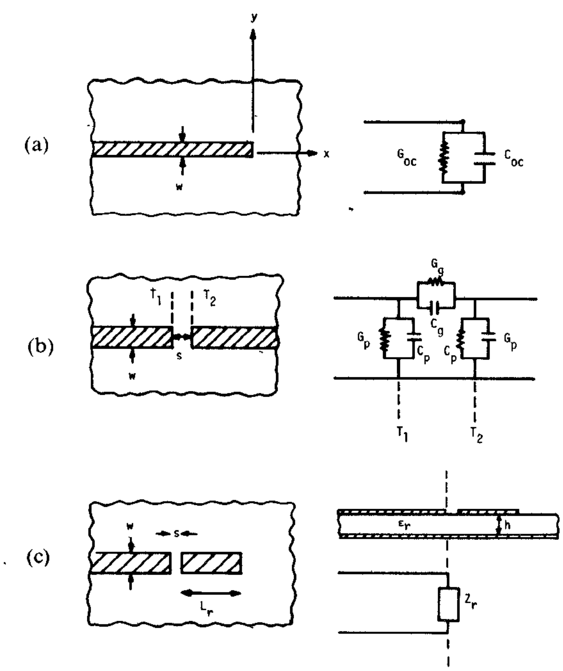

Fig. 1. Microstrip discontinuities and equivalent circuits. (a) Open-circuit microstrip line. (b) Microstrip gap. (c) Coupled microstrip resonator.

Manuscript received March 13, 1985; revised May 31, 1985. This research was supported in part by the U.S. Army under Research Contract DAAG 29-84-K-0067, and in part by the Northrop Corp. under Research Grant 84-110-1006.

P. B. Katehi is with the Department of Electrical Engineering and Computer Science, University of Michigan, Ann Arbor, Michigan 48109.

N. G. Alexopoulos is with the Electrical Engineering Department, University of California, Los Angeles, CA 90024.

0018-9480/85/1000-1029$01.00 ©1985 IEEE

tinuity's radiation conductance in the equivalent circuits, it yields results which at low frequencies are in good agreement with previously published data [5]. However, a comparison of the quasi-statically obtained results with those of the dynamic model developed in this paper shows the inadequacy of the quasi-static approach.

II. Analytical Formulation

A. Current Distribution Evaluation

The current distribution on the transmission-line sections for the discontinuities considered here radiates an electric field given by Pocklington's integral equation

$$\vec{E}(\vec{r}) = \iint_S \bar{\bar{G}}(\vec{r}/\vec{r}')\cdot\vec{J}(\vec{r}')\, ds' \quad (1)$$

where $\vec{E}(\vec{r})$ is the total electric field at the point $\vec{r} = (r,\theta,\phi)$, $\bar{\bar{G}}(\vec{r}/\vec{r}')$ is the dyadic Green's function and $\vec{J}(\vec{r}')$ is the unknown current distribution at the point $\vec{r}' = (r',\theta' = \pi/2,\phi')$. The dyadic Green's function is given by the expression

$$\bar{\bar{G}}(\vec{r}/\vec{r}') = \int_0^\infty \left[k_0^2\bar{\bar{I}} + \overline{\nabla\nabla}\right]\cdot\left(J_0(\lambda|\vec{r}-\vec{r}'|)\bar{\bar{F}}(\lambda)\right) d\lambda \quad (2)$$

with $\bar{\bar{I}}$ the unit dyadic, $k_0 = 2\pi/\lambda_0$, and $\bar{\bar{F}}(\lambda)$ a known dyadic function of the form

$$\bar{\bar{F}}(\lambda) = \frac{\bar{\bar{A}}(\lambda,\epsilon_r,h)}{f_1(\lambda,\epsilon_r,h)f_2(\lambda,\epsilon_r,h)}. \quad (3)$$

In (3), ϵ_r is the relative dielectric constant of the substrate, h is the substrate thickness, and f_1, f_2 are analytic functions of their variables [29], [30].

The integrand in (2) has poles whenever either one of the functions $f_1(\lambda,\epsilon_r,h), f_2(\lambda,\epsilon_r,h)$ becomes zero. The contribution from these poles gives the field propagating in the substrate in the form of TE or TM surface waves [30]. Particularly, the zeros of $f_1(\lambda,\epsilon_r,h)$ correspond to TE surface waves, while the zeros of $f_2(\lambda,\epsilon_r,h)$ to TM surface waves.

Since the widths of the microstrip sections are fractions of the wavelength in the dielectric, it can be assumed that the currents are unidirectional and parallel to the x-axis. Therefore, the current vector in (1) may be written in the form

$$\vec{J}(\vec{r}') = \hat{x}f(x')g(y') \quad (4)$$

where $f(x')$ is an unknown function of x' and $g(y')$ is assumed to be of the form

$$g(y') = \frac{2}{w_e\pi}\left\{1-\left(\frac{2y'}{w_e}\right)^2\right\}^{-1/2}. \quad (5)$$

In (5), w_e is the effective strip width given by $w_e = w + 2\delta$, where δ is the excess half-width and it accounts for fringing effects due to conductor thickness. Formulas for effective width exist in the literature [25], [26] and they have been adopted in this formulation [28].

In order to solve (1) for the current density $\vec{J}$, the method of moments is employed. Each section of the microstrip is divided into a number of segments, and the current is written as a finite sum

$$\vec{J}(\vec{r}') = \hat{x}g(y')\sum_{n=1}^{N} I_n f_n(x') \quad (6)$$

where N is the total number of segments considered and the expansion functions $f_n(x')$ have been chosen to be piecewise sinusoidal functions given by

$$f_n(x') = \begin{cases} \dfrac{\sin[k_0(x'-x_{n-1})]}{\sin(k_0 l_x)}, & x_{n-1} \le x' \le x_n \\ \dfrac{\sin[k_0(x_{n+1}-x')]}{\sin(k_0 l_x)}, & x_n \le x' \le x_{n+1} \\ 0, & \text{otherwise} \end{cases} \quad (7)$$

with l_x being the length of each subsection.

If the electric field is projected along the axis $y=0$, $z=0$ using as weighting functions the basis functions (Galerkin's method), (1) will reduce to a matrix equation of the form

$$\underset{N\times N}{[Z_{mn}]}\ \underset{(N\times 1)}{[I_n]} = \underset{(N\times 1)}{[V_m]} \quad (8)$$

where $[I_n]$ is the vector of unknown coefficients and $[V_m]$ is the excitation vector which depends on the impressed feed model. $[Z_{mn}]$ is the impedance matrix with elements given by

$$Z_{mn} = \delta(y)\delta(z)\int_{-w/2}^{w/2}\frac{dy'}{\left[1-\left(\frac{2y'}{w_e}\right)^2\right]^{1/2}} \cdot\int_C dx\int_C dx'\left\{k_0^2F_{xx} + \frac{\partial^2}{\partial x^2}(F_{xx}-F_{zx})\right\}f_m(x)f_n(x') \quad (9)$$

where

$$F_{xx} = 2\left(\frac{j\omega\mu_0}{4\pi k_0^2}\right)\int_0^\infty\left(\frac{\sinh(uh)}{f_1(\lambda,\epsilon_r,h)}\right)J_0(\lambda\rho)e^{-u_0t}\,d\lambda \quad (10)$$

and

$$F_{zx} = 2\left(\frac{j\omega\mu_0}{4\pi k_0^2}\right)(\epsilon_r-1)\int_0^\infty\left(\frac{u_0\cosh(uh)}{f_1(\lambda,\epsilon_r,h)}\right)\left(\frac{\sinh(uh)}{f_2(\lambda,\epsilon_r,h)}\right)\cdot J_0(\lambda\rho)e^{-u_0t}\,d\lambda. \quad (11)$$

In (9) and (10)

$$u_0 = \left[\lambda^2 - k_0^2\right]^{1/2} \quad u = \left[\lambda^2 - \epsilon_r k_0^2\right]^{1/2} \quad (12)$$

$$f_1(\lambda,\epsilon_r,h) = u_0\sinh(uh) + u\cosh(uh) \quad (13)$$

$$f_2(\lambda,\epsilon_r,h) = \epsilon_r u_0\cosh(uh) + u\sinh(uh) \quad (14)$$

and

$$\rho = \left[(x-x')^2 + (y-y')^2\right]^{1/2}. \quad (15)$$

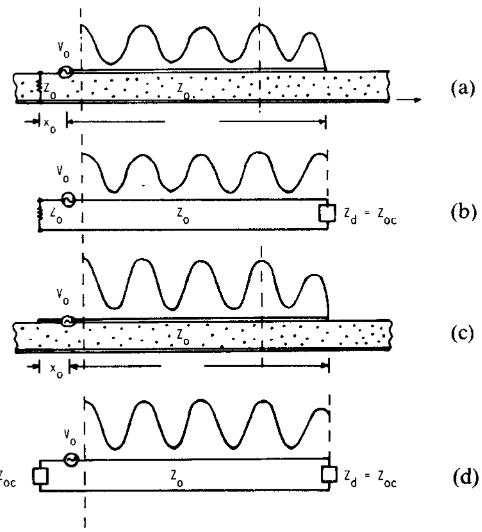

Fig. 2. Modeling of the excitation mechanism for a microstrip transmission line.

Using this form for the evaluation of the elements of the impedance matrix, one can solve the matrix equation shown in (8) to find the unknown coefficients for the current.

B. Excitation Mechanism — Equivalent Impedance

One difficulty always encountered in this type of problem is the implementation of a practical excitation mechanism which can be included in the mathematical modeling. In most applications, the microstrip line is kept as close to the ground as possible and is excited by a coaxial line of the same characteristic impedance. As a result, a unimodal field is excited under the transmission line, reflection at the excitation end is minimized, and the current distribution on the line beyond an appropriate reference plane forms standing waves of a transverse electromagnetic (TEM)-like mode. Thus, this microstrip line can be approximated by an ideal transmission line of the same characteristic impedance Z_0 terminated to an unknown equivalent impedance Z_d (see Fig. 2). It can be shown (see Appendix A) that the reflection coefficient does not change in amplitude and phase if the coaxial line is substituted with a voltage gap generator and the line is left open at the excitation end (see Fig. 2(c)). This excitation mechanism is adopted for the application of moments method in the solution of Pocklington's integral equation and results in an excitation vector $[V_m] = [\delta_{im}]$ with

$$\delta_{im} = \begin{cases} 1 & \text{at the position of the gap generator } (x_i = x_m) \\ 0 & \text{everywhere else } (x_i \neq x_m) \end{cases}.$$

The equivalent ideal transmission line for this type of excitation is shown in Fig. 2(d) where $Z_d = Z_{oc}$ for the case of an open-end microstrip discontinuity. The quasi-TEM mode considered has a wavelength λ_g equal to the dominant spatial frequency of the amplitude of the current which is derived by the method of moments.

If the origin of the x coordinate is taken at the position of Z_d, then the equivalent impedance, normalized with respect to the characteristic impedance, is given by [28]

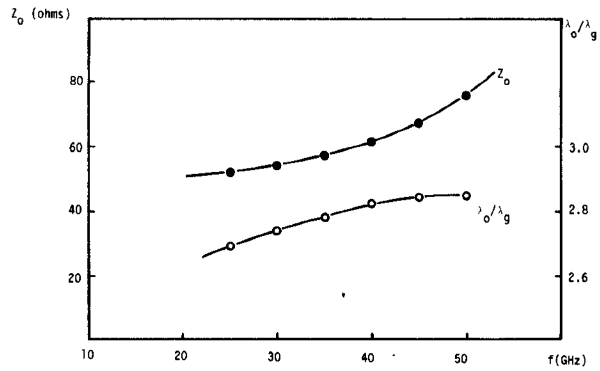

Fig. 3. Characteristic impedance Z_0 and guide wavelength $\lambda_g/\lambda_0$of a microstrip line as a function of frequency ($\epsilon_r = 9.6, w/h = 1, h = 0.6$ mm).

$$Z_d = \frac{1+\Gamma(0)}{1-\Gamma(0)} \tag{16}$$

where

$$\Gamma(0) = -\frac{SWR-1}{SWR+1} e^{j\beta|x_{\max}|} \tag{17}$$

and $x_{\max}$ is the position of a maximum.

From (16) and (17), one can see that the accurate determination of equivalent circuits for different discontinuities depends on the accuracy of evaluating the characteristic impedance Z_0 and guided wavelength $\lambda_g(\beta = 2\pi/\lambda_g)$. The characteristic impedance of the transmission line of Fig. 2(d) is given by (see Appendix B)

$$Z_0 = \frac{1}{|I_{\max}|} \left| \frac{Z_{oc}}{1-Z_{oc}} \right| \cdot \left| e^{j\beta|x_{\max}|} + \frac{1-Z_{oc}}{1+Z_{oc}} e^{-j\beta|x_{\max}|} \right| \tag{18}$$

where $x_{\max}$ is the position of a maximum and $|I_{\max}|$ is the maximum amplitude of the current. Z_{oc} is the normalized equivalent impedance of an open-circuited microstrip line of length $l = (n/2)\lambda_g (n \geq 8)$ and the gap generator is placed at a position $\lambda_g/4$ from one end. The characteristic impedance and guided wavelength are shown as functions of frequency in Fig. 3. These results are in excellent agreement with already existing data [25].

III. Numerical Results

A. Microstrip Open-Circuit Discontinuity

The equivalent circuit from an open-end discontinuity, as shown in Fig. 1, consists of a capacitance C_{oc} in parallel with a conductance G_{oc}, which is proportional to radiation losses. Using the method presented previously, values for the normalized capacitance C_{oc}/w in pF/m and for the conductance G_{oc} (in mmhos) are plotted as functions of frequency for a microstrip line with $w/h = 1$ on a 0.6-mm Alumina substrate (see Fig. 4). From these data, one can conclude that the radiation conductance increases with frequency while the capacitance decreases.

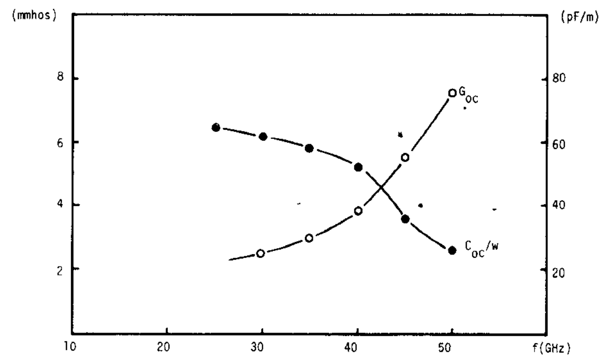

Fig. 4. Radiation conductance G_{oc} and normalized capacitance C_{oc}/w of an open-circuited microstrip line as functions of frequency ($\epsilon_r = 9.6, w/h = 1, h = 0.6$ mm).

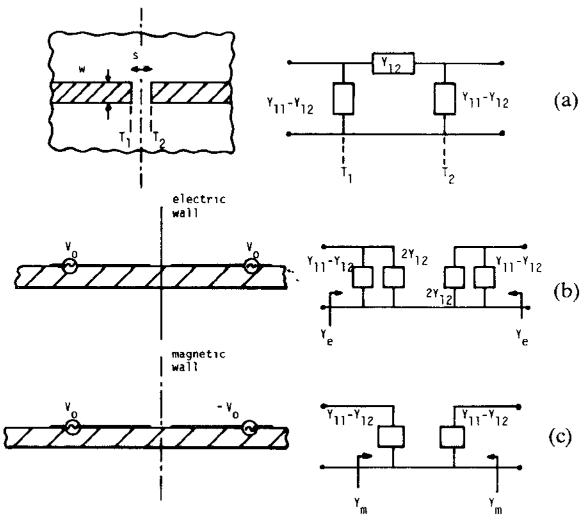

Fig. 5. Gap discontinuity and equivalent circuits.

B. Microstrip Gap Discontinuity

The equivalent circuit for a microstrip gap is shown in Fig. 1. For the evaluation of G_p, C_p, G_g, and C_g, both sections of the microstrip are excited by gap generators which are either in phase (see Fig. 5(a)) or out of phase (Fig. 5(c)). The former case is equivalent to the presence of a magnetic wall in the middle of the gap, while the latter to an electric wall at the same position. The equivalent circuits for these two excitations are shown in Fig. 5(b) and (c) and give

$$Y_e = G_e + j\omega C_e = Y_{11} + Y_{12} \tag{19}$$

and

$$Y_m = G_m + j\omega C_m = Y_{11} - Y_{12} \tag{20}$$

where Y_e, Y_m are the equivalent normalized admittances for the case of the electric and magnetic wall, respectively. From (19) and (20), the conductances and capacitances of a p-type equivalent circuit are given by

$$G_p = G_m \tag{21}$$

$$C_p = C_m \tag{22}$$

$$G_g = \tfrac{1}{2}(G_e - G_m) \tag{23}$$

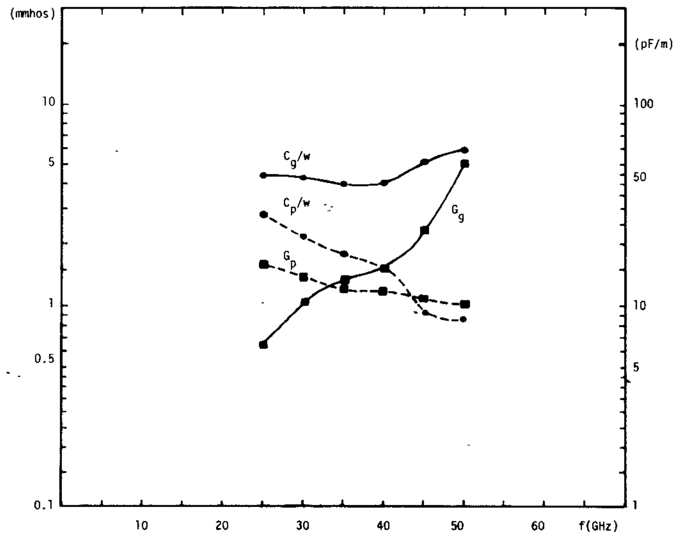

Fig. 6. Gap-discontinuity radiation conductances G_g, G_p, and normalized capacitances C_g/w, C_p/w as functions of frequency ($\epsilon_r = 9.6, w/h = 1, h = 0.6$ mm, $s/h = 0.3762$).

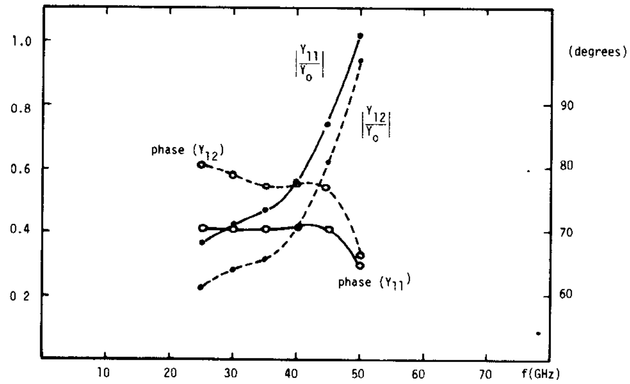

Fig. 7. Gap-discontinuity admittance matrix elements as functions of frequency ($\epsilon_r = 9.6, w/h = 1, h = 0.6$ mm, $s/h = 0.3762$).

and

$$C_g = \tfrac{1}{2}(C_e - C_m) \tag{24}$$

Values of G_p, C_p, G_g, and C_g are plotted as functions of frequency for a microstrip line with $w/h = 1$ on a 0.6-mm Alumina substrate (Fig. 6). From the values for the gap and open-end conductances (Figs. 4 and 6), one can see that as the frequency increases, the radiation losses become higher and, therefore, the inter-circuit coupling through space and surface waves becomes a dominant factor in the design of printed circuits. From (19)–(24), the elements of the admittance matrix of the discontinuity considered as a two port can be found in amplitude and phase as functions of frequency (see Fig. 7).

C. Excess Length and Equivalent Capacitances

Another method of deriving equivalent circuits is based on the evaluation of excess length. The method developed here results in values for the excess length in such a way so as to take into account dispersion and radiation losses. The dominant reason for loss of accuracy at high frequencies by this method is the way the equivalent capacitance is

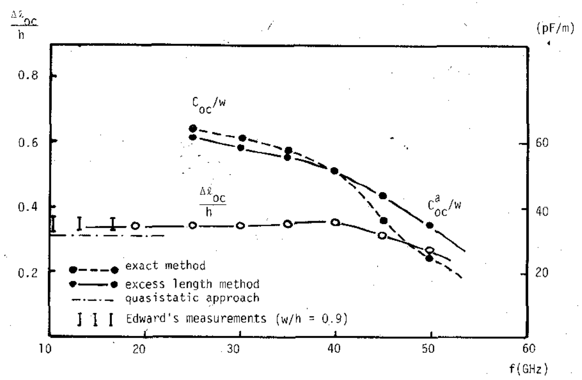

Fig. 8. Open-circuit normalized excess length and normalized capacitances as functions of frequency ($\epsilon_r = 9.6, w/h = 1, h = 0.6$ mm).

evaluated. The excess length Δl_d is measured from the standing waves of the amplitude of the computed current

$$\Delta l_d = \frac{\lambda_g}{4} - d_{\max} \tag{25}$$

where λ_g is the guided wavelength and $d_{\max}$ is the position of the first maximum of the current amplitude from the open end. The discontinuity capacitance C_d^a is evaluated as a function of Δl_d from the following relation [25]:

$$\frac{C_d^a}{w} = \frac{\Delta l_d}{h} \sqrt{\epsilon_{\text{eff}}} \frac{1}{Z_0} \frac{h}{w} \tag{26}$$

where ϵ_{eff} is the effective dielectric constant and Z_0 the characteristic impedance. Equation (26) gives quasi-static values for the capacitance and, therefore, is accurate for low frequencies only.

In Fig. 8, the open-end normalized equivalent capacitance C_{oc}^a/w in pF/m is plotted as a function of frequency and is compared to the values derived with the exact method. As shown, the values of the two capacitances agree at the lower part of the frequency range and they shift away as the frequency becomes higher. In addition, the capacitances C_p, C_g of the p-type equivalent circuit derived with the two methods are compared and they show a big discrepancy at high frequencies where (25) becomes much less accurate (Fig. 9).

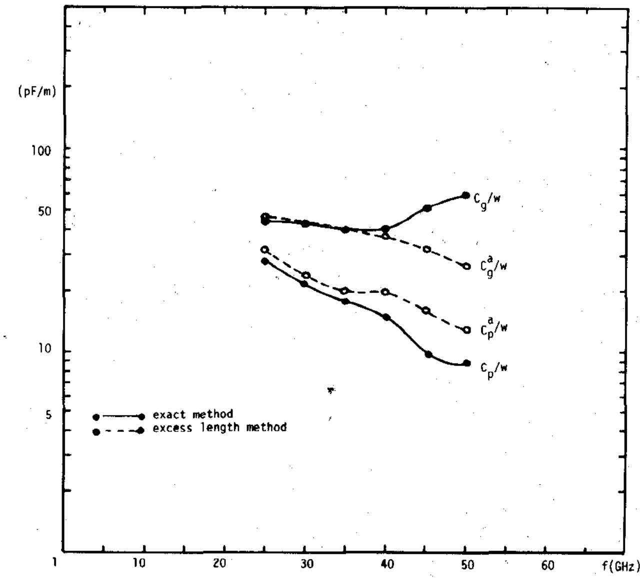

Fig. 9. Gap-discontinuity normalized capacitances C_p/w, C_g/w as functions of frequency ($\epsilon_r = 9.6, w/h = 1, h = 0.6$ mm, $s/h = 0.3762$).

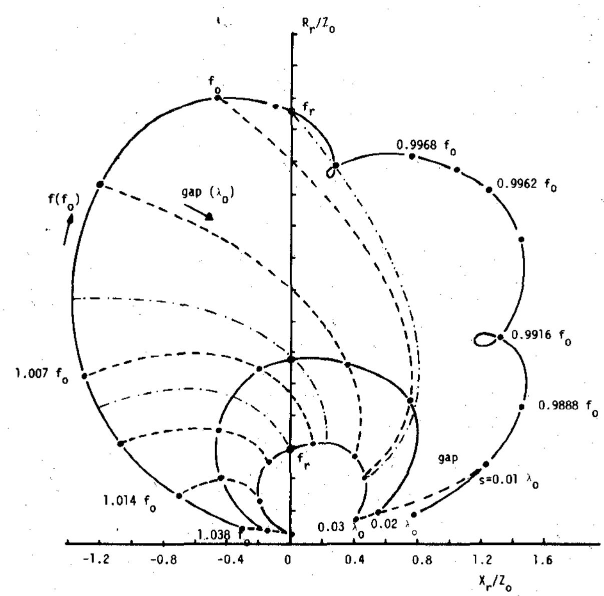

Fig. 10. Normalized equivalent impedance Z_r as a function of frequency f and gap s ($\epsilon_r = 9.9, w/h = 1, h = 0.05\lambda_0, L_r = 0.032\lambda_0$).

D. Coupled Microstrip Resonator

For this discontinuity, the transmission-line model is used for the evaluation of the normalized equivalent impedance Z_r as a function of frequency (see Fig. 1(c)). The normalized impedance Z_r is measured at $\lambda_g/4$ from the open end. In Fig. 10, the real and imaginary parts of Z_r are plotted as functions of frequency for a microstrip line with $w/h = 1$, $t = 0.0001\lambda_0$ on a $0.05\lambda_0$-thick Alumina substrate ($\epsilon_r = 9.9$), and for a gap $s = 0.01\lambda_0$. The lengths have been measured in terms of the free space wavelength λ_0 at a specified frequency f_0. The resonator length L_r varies between $0.031\lambda_0$ and $0.033\lambda_0$. Fig. 10 implies that there exists a particular length L_r for which the VSWR on the transmission line at the resonant frequency f_r becomes unity. Fig. 11(a) indicates that the resonant frequency decreases as the resonator length becomes larger. It is also very interesting to see how the resonant frequency changes as a function of the length of the gap. Fig. 11(b) shows that the resonant frequency increases as the gap becomes larger, while the resonator length was kept constant and equal to $0.032\lambda_0$.

IV. Conclusion

The representation of microstrip discontinuities by equivalent circuits or admittance matrices has been treated by an effective method. The current distribution is computed by the method of moments in the longitudinal direction of the microstrip discontinuities, while in the transverse direction it is chosen as the Maxwell distribution, thus satisfying the edge condition. Upon determining

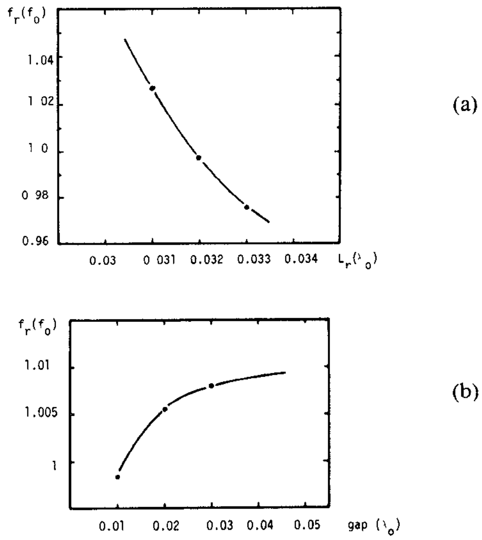

Fig. 11. Resonant frequency f_r as a function of the resonator length and the gap.

the current, a transmission-line model is used for the representation of the unimodal field excited under the microstrip line.

Therefore, the normalized admittance matrix is evaluated in terms of equivalent admittances. This method takes into account dispersion and radiation losses, provides us with equivalent circuits which are an accurate representation of the discontinuities under consideration, and does not have any frequency limitations. Furthermore, this method was compared with results obtained through a quasi-static as well as a waveguide model and was found superior. The accuracy of the method depends on the accuracy of evaluating λ_g, $x_{\max}$, and VSWR. This implies that if more subsections are considered in the method of moments, the error will become smaller. In the present derivations, the estimated error is up to two percent.

Appendix A

The transmission line of Fig. 2(d) is considered and it is assumed that the voltage generator is at the position $x=0$ and that $Z_d \neq Z_{oc}$. The coupled differential equations for the voltage and current in this transmission line are of the form

$$-\frac{dI(x)}{dx} = j\beta Y_0(x) \tag{1A}$$

and

$$-\frac{dV(x)}{dx} = j\beta Z_0 I(x) + V_0\delta(x). \tag{2A}$$

From (1A) and (2A), the differential equation for the current is given by

$$\frac{d^2I(x)}{dx^2} + \beta^2 I(x) = j\beta Y_0 V_0 \delta(x). \tag{3A}$$

From (1A) to (3A), one can conclude that the voltage and the current in this transmission line are of the form

$$I(x<) = B_1 e^{-j\beta x} + B_2 e^{j\beta x} \qquad (x \le 0) \tag{4A}$$

$$I(x>) = A_1 e^{-j\beta x} + A_2 e^{j\beta x} \qquad (x \ge 0) \tag{5A}$$

$$V(x<) = Z_0\left(A_1 e^{-j\beta x} - A_2 e^{j\beta x}\right) \qquad (x \le 0) \tag{6A}$$

and

$$V(x>) = Z_0\left(B_1 e^{-j\beta x} - B_2 e^{j\beta x}\right) \qquad (x \ge 0). \tag{7A}$$

The boundary conditions for this problem are

$$\frac{V(l)}{I(l)} = Z_d \tag{8A}$$

$$\frac{V(-x_0)}{I(-x_0)} = Z_{oc} \tag{9A}$$

$$I(x<) = I(x>) \text{ at } x=0 \tag{10A}$$

and

$$\left.\frac{dI(x>)}{dx}\right|_{x=0} - \left.\frac{dI(x<)}{dx}\right|_{x=0} = j\beta Y_0 V_0. \tag{11A}$$

From (4A) through (11A), one can find that

$$I(x>) = -\frac{1+Z_d}{Z_0}\,\frac{\cos(\beta x_0) - jZ_{oc}\sin(\beta x_0)}{(Z_{oc}-Z_d)\cos[\beta(l-x_0)] + j(Z_{oc}Z_d-1)\sin[\beta(l-x_0)]} \cdot \left\{ e^{-j\beta(x-l)} + \frac{1-Z_{oc}}{1+Z_{oc}} e^{+j\beta(x-l)} \right\}. \tag{12A}$$

From (5A) and (12A), the current reflection coefficient is given by

$$\rho_i = \frac{A_2}{A_1} = \frac{1-Z_{oc}}{1+Z_{oc}} e^{-2j\beta l}. \tag{13A}$$

If the case is considered where the left end of the microstrip line is matched (see Fig. 2(b)), then $B_1 = 0$ and

$$I^m(x>) = -\frac{1}{Z_0}\left\{ e^{-j\beta x} + \frac{1-Z_{oc}}{1+Z_{oc}} e^{j\beta x} e^{-2j\beta l} \right\} \tag{14A}$$

with

$$\rho_i^m = \frac{1-Z_{oc}}{1-Z_{oc}} e^{-2j\beta l}. \tag{15A}$$

From (13A) and (15A), one can conclude that the amplitude and phase of the reflection coefficient do not change when the line is matched at the generator end.

Appendix B

If x_0, l are equal to $\lambda_g/4$ and $\eta(\lambda_g/2)$, then

$$l - x_0 = \frac{2n-1}{4}\lambda_g \tag{B1}$$

and

$$I(x>) = \frac{1+Z_d}{2Z_0}\,\frac{Z_{oc}}{Z_{oc}Z_d - 1}\left\{ e^{-j\beta x} + \frac{1-Z_{oc}}{1+Z_{oc}} e^{j\beta x} \right\}. \tag{B2}$$

At $x = l - x_{\max}$ for $Z_d = Z_{oc}$, the absolute value of the current is given by

$$|I_{\max}| = \frac{1}{Z_0}\left|\frac{Z_{oc}}{Z_{oc}-1}\right|\left|e^{+j\beta|x_{\max}|} + \frac{1-Z_{oc}}{1+Z_{oc}}e^{-j\beta|x_{\max}|}\right| \tag{B3}$$

where $x_{\max}$ is the position of a maximum measured from the equivalent impedance Z_d. Equation (17) is derived from (B3).

References

[1] A. Farrar and A. T. Adams, "Computation of lumped microstrip capacitances by matrix methods: Rectangular sections and end effects," *IEEE Trans. Microwave Theory Tech.*, vol. MTT-19, pp. 495–497, 1971.

[2] M. Maeda, "Analysis of gap in microstrip transmission lines," *IEEE Trans. Microwave Theory Tech.*, vol. MTT-20, 1972.

[3] T. Itoh, R. Mittra, and R. D. Ward, "A method of solving discontinuity problems in microstrip lines," in 1972 *IEEE-GMTT Int. Microwave Symp. Dig.*

[4] P. Silvester and P. Benedek, "Equivalent capacitance of microstrip open circuits," *IEEE Trans. Microwave Theory Tech.* vol. MTT-20, 1972.

[5] P. Benedek and P. Silvester,, "Equivalent capacitance for microstrip gaps and steps," *IEEE Trans. Microwave Theory Tech.*, vol. MTT-20, 1972.

[6] P. Silvester and P. Benedek, "Microstrip discontinuity capacitances for right-angle bends, T-junctions and crossings," *IEEE Trans. Microwave Theory Tech.*, vol. MTT-21, 1973.

[7] R. Horton, "The electrical characterization of a right-angled bend in microstrip line," *IEEE Trans. Microwave Theory Tech.*, vol. MTT-21, 1973.

[8] R. Horton, "Equivalent representation of an abrupt impedance step in microstrip line," *IEEE Trans. Microwave Theory Tech.*, vol. MTT-21, 1973.

[9] A. F. Thompson and A. Gopinath, "Calculation of microstrip discontinuity inductances," *IEEE Trans. Microwave Theory Tech.*, vol. MTT-23, 1975.

[10] A. Gopinath *et al.*, "Equivalent circuit parameters of microstrip step change in width and cross junctions," *IEEE Trans. Microwave Theory Tech.*, vol. MTT-24, 1976.

[11] R. Garg, and I. J. Bahl, "Microstrip discontinuities," *Int. J. Electron.* vol. 45, July 1978.

[12] C. Gupta and A. Gopinath, "Equivalent circuit capacitance of microstrip step change in width," *IEEE Trans. Microwave Theory Tech.*, vol. MTT-25, 1977.

[13] T. Itoh, "Analysis of microstrip resonators," *IEEE Trans. Microwave Theory Tech.*, vol. MTT-22, 1974.

[14] I. Wolf, G. Kompa, and R. Mehran, "Calculation method for microstrip discontinuities and T-junctions," *Electron. Lett.*, vol. 8, 1972.

[15] G. Kompa and R. Mehran, "Planar waveguide model for calculating microstrip components," *Electron. Lett.*, vol. 11, 1975.

[16] G. Kompa, "*S*-matrix computation of microstrip discontinuities with a planar waveguide model," *Arch. Elek. Übertragung.*, vol. 30, 1976.

[17] R. Mehran, "The frequency-dependent scattering matrix of microstrip right-angle bends, T-junctions and crossings," *Arch. Elek. Übertragung.*, vol. 29, 1975.

[18] W. Menzel and I. Wolf, "A method for calculating the frequency dependent properties of microstrip discontinuities," *IEEE Trans. Microwave Theory Tech.*, vol. MTT-25, 1977.

[19] I. W. Stephenson and B. Easter, "Resonant techniques for establishing the equivalent circuits of small discontinuities in microstep," *Electron. Lett.*, vol. 7, pp. 582–584, 1971.

[20] B. Easter, "The equivalent circuits of some microstrip discontinuities," *IEEE Trans. Microwave Theory Tech.*, vol. MTT-23, pp. 655–660, 1975.

[21] J. R. James and A. Henderson, "High frequency behavior of microstrip open-circuit terminations," *Proc. Inst. Elec. Eng., Microwaves, Optics and Acoustics*, vol. 3, no. 4, pp. 205–218, Sept. 1979.

[22] R. Mehran, "Computer-aided design of microstrip filters considering dispersion loss and discontinuity effects," *IEEE Trans. Microwave Theory Tech.*, vol. MTT-27, pp. 239–245, Mar. 1979.

[23] P. B. Katehi and N. G. Alexopoulos, "On the effect of substrate thickness and permittivity on printed circuit dipole properties," *IEEE Trans. Antennas Propagat.*, vol. AP-31, Jan. 1983.

[24] N. G. Alexopoulos, P. B. Katehi, and D. B. Rutledge, "Substrate optimization for integrated circuit antennas," *IEEE Trans. Microwave Theory Tech.*, vol. MTT-31, July 1983.

[25] K. G. Gupta, R. Garg, and I. J. Bahl, *Microstrip Lines and Slotlines.* Dedham, MA: Artech House, 1979.

[26] T. C. Edwards, *Foundations for Microstrip Circuit Design.* New York: Wiley, 1981.

[27] P. B. Katehi and N. G. Alexopoulos, "On the theory of printed circuit antennas for millimeter waves," in Conf. Dig., *Sixth Int. Conf. Infrared and Millimeter Waves*, Dec. 1981, pp. F.2.9–F.2.10.

[28] P. B. Katehi and N. G. Alexopoulos, "On the modeling of electromagnetically coupled microstrip antennas—The printed strip dipole," *IEEE Trans. Antennas Propagat.*, vol. AP-32, Nov. 1984.

[29] P. B. Katehi, "A generalized solution to a class of printed circuit antennas," Ph.D. dissertation, Univ. of California, Los Angeles, 1984.

[30] N. G. Alexopoulos, D. R. Jackson, and P. B. Katehi, "Criteria for nearly omnidirectional radiation patterns for printed antennas," *IEEE Trans. Antennas Propagat.*, vol. AP-33, Feb. 1985.

[31] P. B. Katehi and N. G. Alexopoulos, "Real axis integration of Sommerfeld integrals with applications to printed circuit antennas," *J. Math. Phys.*, vol. 24(3), Mar. 1983.

Pisti B. Katehi was born in Athens, Greeece. She received the B.S.E.E. degree from the National Technical University of Athens, Greece, in 1977 and the M.S.E.E. and Ph.D. degrees from the University of California, Los Angeles in 1981 and 1984, respectively.

She is currently an Assistant Professor in the Department of Electrical Engineering and Computer Science, University of Michigan, Ann Arbor. Her research interests are in the theoretical modeling and measurements of circuit antennas and microstrip integrated-circuit components.

Nicólaos G. Alexópoulos (S'68–M'69–SM'82) was born in Athens, Greece, in 1942. He graduated from the 8th Gymnasium of Athens, Greece, and subsequently obtained the B.S.E.E., M.S.E.E., and Ph.D. degrees from the University of Michigan, Ann Arbor, MI, in 1964, 1967, and 1968, respectively.

He is currently a Professor in the Department of Electrical Engineering, University of California, Los Angeles, the President of NGA Scientific Consultants, and a Consultant with Northrop Corporation's Advanced Systems Division. His current research interests are in electromagnetic theory as it applies in the modeling of integrated-circuit components and printed circuit antennas for microwave and millimeter-wave applications, substrate materials and their effect on integrated-circuit structures and printed antennas, integrated-circuit antenna arrays, and antenna concealment studies. He is the Associate Editor of the IEEE TRANSACTIONS ON ANTENNAS AND PROPAGATION, *Electromagnetics Journal*, and *Alta Frequenza*.